A phase-field model without artificial curvature effect for the crystal growth simulation

Yibao Li [a], Qian Yu [a], Seokjun Ham [b], Soobin Kwak [b], Chaeyoung Lee [b], Junseok Kim [b,*]

[a] *School of Mathematics and Statistics, Xi'an Jiaotong University, Xi'an 710049, China*
[b] *Department of Mathematics, Korea University, Seoul 02841, Republic of Korea*

A R T I C L E   I N F O

A B S T R A C T

In this study, we present a novel phase-field model without artificial curvature effect for the crystal growth simulation. Most phase-field models for dendritic growth are based on the anisotropic Allen–Cahn (AC) equation which models anti-phase domain coarsening in a binary alloy. However, the AC equation intrinsically contains the motion by mean curvature term, i.e., curvature flow, which may have effect on the phases transition. In this work, we remove the artificial curvature effect and propose a novel phase-field model without artificial curvature effect for the dendritic growth simulation. Both two- and three-dimensional numerical tests show that, in the case of the new phase-field model, dendritic growth develops faster than the conventional phase-field model because of the absence of artificial motion by mean curvature effect. In addition, we show that the proposed model has applicability to polycrystal growth.

1. Introduction

Dendritic growth describes a phenomenon where the liquid is transformed into the solid through heat conduction. The simulation of crystal growth is important because of wide applications in material [1–3], climate environment [4] and industry processes [5,6]. The simulation methods of crystal growth include front-tracking, boundary integral, level-set, phase-field [7,8] and cellular automata [9,10], to name a few. Recently, the phase-field method has become popular because of its simplicity in capturing the complex interface by an order parameter without requirement of re-initialization operation [11,12]. Many phase-field models for dendritic growth are based on the anisotropic Allen–Cahn (AC) equation [13–15]. For example, anti-phase domain coarsening in a binary alloy can be modeled by the AC equation:

$$\frac{\partial \phi}{\partial t} = \nabla^2 \phi + \frac{\phi(1-\phi^2)}{\epsilon^2}, \qquad (1)$$

where ϕ is the order parameter with $\phi = 1$ in one phase and $\phi = -1$ in the other phase. The parameter ϵ is related to the interfacial transition thickness between two phases. The AC equation consists of two terms: Laplace diffusion term which is related to the curvature effects and the other nonlinear term which is derived from

the double well potential. However, the Laplace diffusion term intrinsically includes the motion by mean curvature term, i.e., curvature flow [16–18], which may have effect on the evolution dynamics of the model. For example, Takaki and Kato [19] developed a phase-field topology optimization model that removed the mean curvature effects to minimize only the elastic strain energy function rather than the interface energy. This model results in structures with more excellent mechanical property. Subtracting the curvature contribution from a phase-field equation was also used in multiphase fluid flows [20–23] to make the system recover to the equilibrium state. Therefore, the primary motivation of this research is to study the effect on the crystal growth simulation when the mean curvature which we call as the artificial curvature is subtracted. To the authors' knowledge, this is the first study of removing artificial curvature effect from the phase-field model for the crystal growth simulation in two- and three-dimensional spaces.

Many efficient and accurate computational methods for the crystal growth simulations have been developed. Li et al. [24] used a coupled phase field and lattice Boltzmann scheme to numerically simulate the growth of polymer crystal in the flow field. They confirmed that the flow velocities had a significant effect on the crystallization formation and the crystals grew faster in the upstream direction. Wang et al. [25] developed a novel phase-field-lattice Boltzmann equation for dendritic growth with melt fluid flow and thermosolutal convection–diffusion. Shah et al. [26] developed an efficient temporal adaptive method for the dendritic crystal growth. Wu et al. [27] proposed a parallel adaptive multi-

* Corresponding author.
E-mail address: cfdkim@korea.ac.kr (J. Kim).
URL: https://mathematicians.korea.ac.kr/cfdkim/ (J. Kim)

grid method to solve the coupled thermal-solute phase-field problems. Chen et al. [28] considered the sequential nature of the grid correction in multigrid solver for the numerical solution of the rapid solidification of an undercooled binary mixture. Li et al. [29] developed an accurate and efficient numerical scheme for the phase-field based dendritic growth. The difficulty is not only limited in dealing with the traditional phase-field based dendritic crystal growth, but also the artificial curvature term being subtracted which increase the complexity of numerical computation. Kaiser et al. [30] developed a conservative interface-interaction scheme for a sharp-interface framework of liquid-solid phase transition. Zhang et al. [31] performed the 3D phase-field computations of crystal growth using a multilevel thermosolutal phase-field lattice-Boltzmann scheme. Using parallel program and adaptivity grid, they performed the 3D thermosolutal computations to investigate the effect of thermal evolution on the growth of dendrites. Nandi and Sanyasiraju [32] solved the two-phase problems of solidification in complex domains using alternating direction implicit method, which is unconditionally stable.

The main purpose of this study is to present a novel phase-field model without artificial curvature effect for the dendritic growth simulation. Focusing on the effect of artificial curvature term on dendritic growth, we use the simplest numerical method, a fully Euler's scheme to discretize the time and the cell-centered difference method to discretize the space. Many accurate and stable numerical scheme will be further explored in the future. The numerical tests of four-fold and six-fold symmetric crystal growth and polycrystal growth under certain initial conditions will be performed to study the effect of artificial curvature term on dendritic growth.

The paper is organized as follows. In Section 2, the proposed novel phase-field based crystal growth model without the artificial curvature is presented. The numerical solution algorithm is given in Section 3. Various computational tests are done in Section 4. In Section 5, conclusions are derived.

2. Proposed phase-field model

In this section, we present the novel phase-field model without artificial curvature effect for the dendritic growth simulation. First, the conventional phase-field model for the crystal growth can be derived as follows [33,34]:

$$
\epsilon^2(\mathbf{n}) \frac{\partial \phi}{\partial t} = \nabla \cdot (\epsilon^2(\mathbf{n}) \nabla \phi) + [\phi - \lambda U(1-\phi^2)](1-\phi^2) \\
+ \left(|\nabla \phi|^2 \epsilon(\mathbf{n}) \frac{\partial \epsilon(\mathbf{n})}{\partial \phi_x} \right)_x + \left(|\nabla \phi|^2 \epsilon(\mathbf{n}) \frac{\partial \epsilon(\mathbf{n})}{\partial \phi_y} \right)_y,
\tag{2}
$$

$$
\frac{\partial U}{\partial t} = D \nabla^2 U + \frac{1}{2} \frac{\partial \phi}{\partial t}.
\tag{3}
$$

Here ϕ represents the order parameter. We define $\phi = 1$ and $\phi = -1$ in the solid and liquid phases, respectively. $\epsilon(\mathbf{n})$ represents the anisotropic function, $\mathbf{n}$ represents the inward normal unit vector, and $U = c_p(T - T_M)/L$ represents the dimensionless temperature field in which c_p is defined as the specific heat at constant pressure, T_M is defined as the melting temperature and L is defined as the latent heat of fusion. $D = \alpha \tau_0/\epsilon_0^2$ where α is defined as the thermal diffusivity, τ_0 is defined as the characteristic time, and ϵ_0 is defined as the characteristic length. λ represents the dimensionless coupling parameter, is defined as $\lambda = D/a_2$. A normal vector of the interface is defined as (ϕ_x, ϕ_y) and θ that satisfies $\tan \theta = (-\phi_y)/(-\phi_x)$. Then, by replacing $\epsilon(\mathbf{n})$ with $\epsilon(\theta) =$
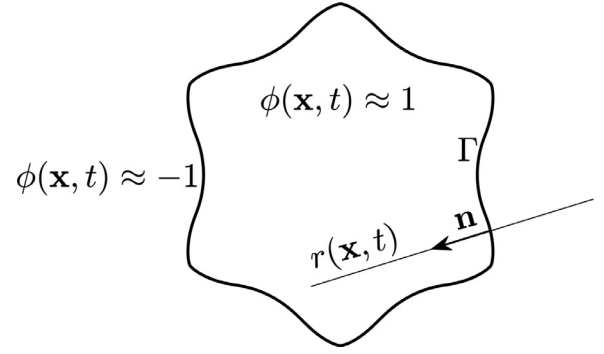

Fig. 1. Schematic illustration of Γ, $r(\mathbf{x}, t)$, and $\mathbf{n}$.

$\epsilon_0(1 + \epsilon_k \cos(k\theta))$, Eq. (2) becomes

$$
\left(|\nabla \phi|^2 \epsilon(\theta) \frac{\partial \epsilon(\theta)}{\partial \phi_x} \right)_x = \left((\phi_x^2 + \phi_y^2) \epsilon(\theta) \epsilon'(\theta) \left(-\frac{\phi_y}{\phi_x^2 + \phi_y^2} \right) \right)_x \\
= -\left(\epsilon'(\theta) \epsilon(\theta) \phi_y \right)_x,
$$

$$
\left(|\nabla \phi|^2 \epsilon(\theta) \frac{\partial \epsilon(\theta)}{\partial \phi_y} \right)_y = \left((\phi_x^2 + \phi_y^2) \epsilon(\theta) \epsilon'(\theta) \left(\frac{\phi_x}{\phi_x^2 + \phi_y^2} \right) \right)_x \\
= \left(\epsilon'(\theta) \epsilon(\theta) \phi_x \right)_y.
$$

Hence, we can rewrite Eq. (2) as follows:

$$
\epsilon^2(\theta) \frac{\partial \phi}{\partial t} = \nabla \cdot (\epsilon^2(\theta) \nabla \phi) + [\phi - \lambda U(1-\phi^2)](1-\phi^2) \\
- \left(\epsilon'(\theta) \epsilon(\theta) \phi_y \right)_x + \left(\epsilon'(\theta) \epsilon(\theta) \phi_x \right)_y
\tag{4}
$$

$$
= \underbrace{\nabla \cdot (\epsilon^2(\theta) \nabla \phi) + \phi(1-\phi^2)}_{I} \\
\underbrace{-\lambda U(1-\phi^2)^2 - \left(\epsilon'(\theta) \epsilon(\theta) \phi_y \right)_x + \left(\epsilon'(\theta) \epsilon(\theta) \phi_x \right)_y}_{G},
\tag{5}
$$

where I and G are phase-preserving and growth terms, respectively. In the phase-field model for the crystal growth, the I term enforces the phase-field shape to have approximately local equilibrium state, which implies we have a hyperbolic tangent profile across interface transition layer. The term G makes the crystal anisotropically grow according to $\epsilon(\theta)$. However, the I term includes an artificial curvature term which reduces the growth of crystal. Now, we identify the artificial curvature term, $\epsilon^2(\theta)|\nabla \phi|\nabla \cdot (\nabla \phi/|\nabla \phi|)$ and remove it from the original governing equation to derive the proposed model. For simplicity, we consider the derivation of the curvature term in two-dimensional space, $\mathbf{x} = (x, y)$. Let $r(\mathbf{x}, t) = \text{dist}(\mathbf{x}, \Gamma)\text{sgn}(\phi(\mathbf{x}, t))$ be a local coordinate, where Γ and $\text{sgn}(\cdot)$ are a zero-level set of ϕ and a sign function, respectively. Let $\mathbf{n} = \nabla \phi/|\nabla \phi|$ be the inward unit normal vector on interface transition layer [35]. Figure 1 shows the schematic illustration of $r(\mathbf{x}, t)$ and $\mathbf{n}$.

Then, we have the following derivation for the Laplacian operator.

$$
\nabla^2 \phi = \nabla \cdot \nabla \phi = \nabla \cdot (|\nabla \phi| \mathbf{n}) = \nabla \cdot ((\nabla \phi \cdot \mathbf{n})\mathbf{n}) = \nabla \cdot (\phi_r \mathbf{n}) \\
= \nabla \phi_r \cdot \mathbf{n} + \phi_r \nabla \cdot \mathbf{n} = (\nabla \phi)_r \cdot \mathbf{n} + \phi_r \nabla \cdot \mathbf{n} \\
= (\phi_r \mathbf{n})_r \cdot \mathbf{n} + \phi_r \nabla \cdot \mathbf{n} = (\phi_{rr} \mathbf{n} + \phi_r \mathbf{n}_r) \cdot \mathbf{n} + \phi_r \nabla \cdot \mathbf{n} \\
= \phi_{rr} + |\nabla \phi| \nabla \cdot (\nabla \phi/|\nabla \phi|).
\tag{6}
$$

In the conventional phase-field model (2), it contains the following AC type equation [17], a governing equation for the motion by mean curvature:

$$
\epsilon^2(\mathbf{n}) \frac{\partial \phi}{\partial t} = \epsilon^2(\mathbf{n}) \nabla^2 \phi + \phi(1-\phi^2).
\tag{7}
$$

Here, $\nabla^2\phi$ in Eq. (7) can be replaced by Eq. (6). Then we have

$$\epsilon^2(\mathbf{n})\frac{\partial\phi}{\partial t} = \epsilon^2(\mathbf{n})\phi_{rr} + \epsilon^2(\mathbf{n})|\nabla\phi|\nabla\cdot\left(\frac{\nabla\phi}{|\nabla\phi|}\right) + \phi(1-\phi^2). \quad (8)$$

According to the dynamics of the AC equation, $\epsilon^2(\mathbf{n})\phi_{rr} + \phi(1-\phi^2) \approx 0$ when $\epsilon(\mathbf{n})$ is close to a constant. Therefore, if we want to use the phase-field model to preserve the interface shapes while applying other factors such as growth and anisotropic evolution, then $\epsilon^2(\theta)|\nabla\phi|\nabla\cdot(\nabla\phi/|\nabla\phi|)$ in Eq. (8) becomes an unnecessary term. Hence, it is natural to remove the artificial curvature effect $\epsilon^2(\theta)|\nabla\phi|\nabla\cdot(\nabla\phi/|\nabla\phi|)$ from the phase-field model for dendritic growth.

Finally, we can propose the following phase-field model without artificial curvature effect for the crystal growth simulation by subtracting the artificial curvature term $\epsilon^2(\theta)|\nabla\phi|\nabla\cdot(\nabla\phi/|\nabla\phi|)$ from Eq. (4):

$$\epsilon^2(\theta)\frac{\partial\phi}{\partial t} = \nabla\cdot(\epsilon^2(\theta)\nabla\phi) - \epsilon^2(\theta)|\nabla\phi|\nabla\cdot\left(\frac{\nabla\phi}{|\nabla\phi|}\right)$$
$$+[\phi - \lambda U(1-\phi^2)](1-\phi^2)$$
$$-\left(\epsilon'(\theta)\epsilon(\theta)\phi_y\right)_x + \left(\epsilon'(\theta)\epsilon(\theta)\phi_x\right)_y, \quad (9)$$

$$\frac{\partial U}{\partial t} = D\nabla^2 U + \frac{1}{2}\frac{\partial\phi}{\partial t}. \quad (10)$$

3. Numerical solution

Focusing on the novel proposed model and facilitating new comers to this novel model, we use a fully explicit Euler's method to discretize the governing Eqs. (9) and (10). Considering a computational domain $\Omega = (L_x, R_x) \times (L_y, R_y)$, let N_x and N_y be integers, $h = (R_x - L_x)/N_x$ be a grid size, and $\Omega_h = \{(x_i, y_j) : x_i = L_x + (i - 0.5)h, \; y_j = L_y + (j - 0.5)h, \; 1 \le i \le N_x, \; 1 \le j \le N_y\}$ be the discrete domain. Let ϕ_{ij}^n and U_{ij}^n be numerical solutions of $\phi(x_i, y_j, n\Delta t)$ and $U(x_i, y_j, n\Delta t)$, respectively, where Δt is the time step. The cell-centered difference scheme of the spatial discretization is used. Then, we can obtain the fully discrete equations as follows:

$$\epsilon^2(\theta_{ij}^n)\frac{\phi_{ij}^{n+1} - \phi_{ij}^n}{\Delta t} = \left[\nabla_d\cdot(\epsilon^2(\theta)\nabla_d\phi)\right]_{ij}^n$$
$$-\left[\epsilon^2(\theta)|\nabla_d\phi|\nabla_d\cdot\left(\frac{\nabla_d\phi}{|\nabla_d\phi|}\right)\right]_{ij}^n \quad (11)$$

$$+[\phi_{ij}^n - \lambda U_{ij}^n(1-(\phi_{ij}^n)^2)][1-(\phi_{ij}^n)^2]$$
$$-\left[D_x\left(\epsilon'(\theta)\epsilon(\theta)D_y\phi\right)\right]_{ij}^n + \left[D_y\left(\epsilon'(\theta)\epsilon(\theta)D_x\phi\right)\right]_{ij}^n,$$

$$\frac{U_{ij}^{n+1} - U_{ij}^n}{\Delta t} = D\nabla_d^2 U_{ij}^n + \frac{\phi_{ij}^{n+1} - \phi_{ij}^n}{2\Delta t}. \quad (12)$$

To compute $\epsilon^2(\theta_{ij}^n)$, we firstly calculate the angle between the normal vector of interface and a reference x-axis by $\theta_{ij}^n = \tan^{-1}\left[(\phi_{i,j-1}^n - \phi_{i,j+1}^n)/(\phi_{i-1,j}^n - \phi_{i+1,j}^n)\right]$. The other terms in the right hand side of Eq. (11) are discretized as follows:

$$\left[\nabla_d\cdot(\epsilon^2(\theta)\nabla_d\phi)\right]_{ij}^n$$
$$= \frac{\epsilon^2(\theta_{i,j+\frac{1}{2}}^n)\left(\phi_{i,j+1}^n - \phi_{ij}^n\right) - \epsilon^2(\theta_{i,j-\frac{1}{2}}^n)\left(\phi_{ij}^n - \phi_{i,j-1}^n\right)}{h^2}$$
$$+ \frac{\epsilon^2(\theta_{i+\frac{1}{2},j}^n)\left(\phi_{i+1,j}^n - \phi_{ij}^n\right) - \epsilon^2(\theta_{i-\frac{1}{2},j}^n)\left(\phi_{ij}^n - \phi_{i-1,j}^n\right)}{h^2},$$

$$\left[D_x\left(\epsilon'(\theta)\epsilon(\theta)D_y\phi\right)\right]_{ij}^n$$

$$= \frac{\epsilon'(\theta_{i+\frac{1}{2},j})\epsilon(\theta_{i+\frac{1}{2},j})\left(\phi_{i+1,j+1}^n - \phi_{i+1,j-1}^n + \phi_{i,j+1}^n - \phi_{i,j-1}^n\right)}{4h^2}$$
$$- \frac{\epsilon'(\theta_{i-\frac{1}{2},j})\epsilon(\theta_{i-\frac{1}{2},j})\left(\phi_{i,j+1}^n - \phi_{i,j-1}^n + \phi_{i-1,j+1}^n - \phi_{i-1,j-1}^n\right)}{4h^2},$$

$$\left[D_y\left(\epsilon'(\theta)\epsilon(\theta)D_x\phi\right)\right]_{ij}^n$$

$$= \frac{\epsilon'(\theta_{i,j+\frac{1}{2}})\epsilon(\theta_{i,j+\frac{1}{2}})\left(\phi_{i+1,j+1}^n - \phi_{i-1,j+1}^n + \phi_{i+1,j}^n - \phi_{i-1,j}^n\right)}{4h^2}$$
$$- \frac{\epsilon'(\theta_{i,j-\frac{1}{2}})\epsilon(\theta_{i,j-\frac{1}{2}})\left(\phi_{i+1,j}^n - \phi_{i-1,j}^n + \phi_{i+1,j-1}^n - \phi_{i-1,j-1}^n\right)}{4h^2},$$

where $\epsilon'(\theta) = -k\epsilon_0\epsilon_k\sin(k\theta)$ and

$$\theta_{i+\frac{1}{2},j}^n = \tan^{-1}\left(\frac{\phi_{i+1,j-1}^n - \phi_{i+1,j+1}^n + \phi_{i,j-1}^n - \phi_{i,j+1}^n}{4(\phi_{ij}^n - \phi_{i+1,j}^n)}\right),$$

$$\theta_{i-\frac{1}{2},j}^n = \tan^{-1}\left(\frac{\phi_{i,j-1}^n - \phi_{i,j+1}^n + \phi_{i-1,j-1}^n - \phi_{i-1,j+1}^n}{4(\phi_{i-1,j}^n - \phi_{ij}^n)}\right),$$

$$\theta_{i,j+\frac{1}{2}}^n = \tan^{-1}\left(\frac{4(\phi_{ij}^n - \phi_{i,j+1}^n)}{\phi_{i-1,j+1}^n - \phi_{i+1,j+1}^n + \phi_{i-1,j}^n - \phi_{i+1,j}^n}\right),$$

$$\theta_{i,j-\frac{1}{2}}^n = \tan^{-1}\left(\frac{4(\phi_{i,j-1}^n - \phi_{ij}^n)}{\phi_{i-1,j}^n - \phi_{i+1,j}^n + \phi_{i-1,j-1}^n - \phi_{i+1,j-1}^n}\right).$$

The term $\left[\epsilon^2(\theta)|\nabla_d\phi|\nabla_d\cdot(\nabla_d\phi/|\nabla_d\phi|)\right]_{ij}^n$ is defined as follows: $|\nabla_d\phi_{ij}^n| = |\nabla_d\phi^n_{i+\frac{1}{2},j+\frac{1}{2}} + \nabla_d\phi^n_{i+\frac{1}{2},j-\frac{1}{2}} + \nabla_d\phi^n_{i-\frac{1}{2},j+\frac{1}{2}} + \nabla_d\phi^n_{i-\frac{1}{2},j-\frac{1}{2}}|/4$, where $\nabla_d\phi_{i+\frac{1}{2},j+\frac{1}{2}} = (\phi^x_{i+\frac{1}{2},j+\frac{1}{2}}, \phi^y_{i+\frac{1}{2},j+\frac{1}{2}}) = ((\phi_{i+1,j} + \phi_{i+1,j+1} - \phi_{ij} - \phi_{i,j+1})/(2h), (\phi_{i,j+1} + \phi_{i+1,j+1} - \phi_{ij} - \phi_{i+1,j})/(2h))$. Then, we define the discrete curvature term as follows:

$$\nabla_d\cdot\left(\frac{\nabla_d\phi}{|\nabla_d\phi|}\right)_{ij} = \frac{1}{2h}\left(\frac{\phi^x_{i+\frac{1}{2},j+\frac{1}{2}} + \phi^y_{i+\frac{1}{2},j+\frac{1}{2}}}{|\nabla_d\phi_{i+\frac{1}{2},j+\frac{1}{2}}|} + \frac{\phi^x_{i+\frac{1}{2},j-\frac{1}{2}} - \phi^y_{i+\frac{1}{2},j-\frac{1}{2}}}{|\nabla_d\phi_{i+\frac{1}{2},j-\frac{1}{2}}|}\right.$$
$$\left. - \frac{\phi^x_{i-\frac{1}{2},j+\frac{1}{2}} - \phi^y_{i-\frac{1}{2},j+\frac{1}{2}}}{|\nabla_d\phi_{i-\frac{1}{2},j+\frac{1}{2}}|} - \frac{\phi^x_{i-\frac{1}{2},j-\frac{1}{2}} + \phi^y_{i-\frac{1}{2},j-\frac{1}{2}}}{|\nabla_d\phi_{i-\frac{1}{2},j-\frac{1}{2}}|}\right).$$

According to Eqs. (11) and (12), combining the discretization of the Laplacian operator for temperature $\nabla_d^2 U_{ij}^n = (U_{i+1,j}^n + U_{i-1,j}^n + U_{i,j+1}^n + U_{i,j-1}^n - 4U_{ij}^n)/h^2$ and all above discrete terms, we can update the numerical solutions in explicit forms as follows:

$$\phi_{ij}^{n+1} = \phi_{ij}^n + \left\{\left[\nabla_d\cdot(\epsilon^2(\theta)\nabla_d\phi)\right]_{ij}^n\right.$$
$$-\left[\epsilon^2(\theta)|\nabla_d\phi|\nabla_d\cdot\left(\frac{\nabla_d\phi}{|\nabla_d\phi|}\right)\right]_{ij}^n$$
$$+[\phi_{ij}^n - \lambda U_{ij}^n(1-(\phi_{ij}^n)^2)][1-(\phi_{ij}^n)^2]$$
$$\left. -\left[D_x\left(\epsilon'(\theta)\epsilon(\theta)D_y\phi\right)\right]_{ij}^n + \left[D_y\left(\epsilon'(\theta)\epsilon(\theta)D_x\phi\right)\right]_{ij}^n\right\}\Bigg/$$
$$\left(\frac{\epsilon^2(\theta_{ij}^n)}{\Delta t}\right), \quad (13)$$

$$U_{ij}^{n+1} = U_{ij}^n + \Delta t D\nabla_d^2 U_{ij}^n + \frac{\phi_{ij}^{n+1} - \phi_{ij}^n}{2}. \quad (14)$$

It should be noted that Eqs. (13) and (14) are solved with the homogeneous Neumann boundary conditions.

3.1. Three-dimensional method

We consider the solution algorithm in the three-dimensional space. The governing equation for the three-dimensional phase-

field model without artificial curvature effect for crystal growth simulation is given as:

$$\epsilon^2(\phi)\frac{\partial \phi}{\partial t} = \nabla \cdot (\epsilon^2(\phi)\nabla \phi) - \epsilon^2(\phi)|\nabla \phi|\nabla \cdot \left(\frac{\nabla \phi}{|\nabla \phi|}\right)$$
$$+ [\phi - \lambda U(1-\phi^2)](1-\phi^2)$$
$$+ \left(|\nabla \phi|^2 \epsilon(\phi)\frac{\partial \epsilon(\phi)}{\partial \phi_x}\right)_x + \left(|\nabla \phi|^2 \epsilon(\phi)\frac{\partial \epsilon(\phi)}{\partial \phi_y}\right)_y$$
$$+ \left(|\nabla \phi|^2 \epsilon(\phi)\frac{\partial \epsilon(\phi)}{\partial \phi_z}\right)_z, \tag{15}$$

$$\frac{\partial U}{\partial t} = D\nabla^2 U + \frac{1}{2}\frac{\partial \phi}{\partial t}. \tag{16}$$

Here, $\epsilon(\phi)$ is the anisotropic function [36] for cubic symmetry which is defined as:

$$\epsilon(\phi) = (1 - 3\delta_4)\left(1 + \frac{4\delta_4}{1-3\delta_4}\frac{\phi_x^4 + \phi_y^4 + \phi_z^4}{|\nabla \phi|^4}\right).$$

Now, using the fully explicit Euler's method, we discretize Eqs. (15) and (16) on a three-dimensional domain $\Omega = (L_x, R_x) \times (L_y, R_y) \times (L_z, R_z)$. Let N_x, N_y, and N_z be positive integers, $h = (R_x - L_x)/N_x$ be the uniform mesh size, and $\Omega_h = \{(x_i, y_j, z_k) : x_i = L_x + (i-0.5)h, \; y_j = L_y + (j-0.5)h, \; z_k = L_z + (k-0.5)h, \; 1 \le i \le N_x, \; 1 \le j \le N_y, \; 1 \le j \le N_z\}$ be the discrete space. Let $\phi_{ijk}^n = \phi(x_i, y_j, z_k, n\Delta t)$ and $U_{ijk}^n = U(x_i, y_j, z_k, n\Delta t)$. Here, we also use the cell-centered difference scheme for the spatial discretization. Finally the fully discrete governing equations are obtained as follows:

$$\epsilon^2(\phi_{ijk}^n)\frac{\phi_{ijk}^{n+1} - \phi_{ijk}^n}{\Delta t} = \left[\nabla_d \cdot (\epsilon^2(\phi)\nabla_d \phi)\right]_{ijk}^n$$
$$- \left[\epsilon^2(\phi)|\nabla_d \phi|\nabla_d \cdot \left(\frac{\nabla_d \phi}{|\nabla_d \phi|}\right)\right]_{ijk}^n \tag{17}$$

$$+ [\phi_{ijk}^n - \lambda U_{ijk}^n(1 - (\phi_{ijk}^n)^2)][1 - (\phi_{ijk}^n)^2]$$
$$+ \left[\left(|\nabla \phi|^2 \epsilon(\phi)\frac{\partial \epsilon(\phi)}{\partial \phi_x}\right)_x\right]_{ijk}^n + \left[\left(|\nabla \phi|^2 \epsilon(\phi)\frac{\partial \epsilon(\phi)}{\partial \phi_y}\right)_y\right]_{ijk}^n$$
$$+ \left[\left(|\nabla \phi|^2 \epsilon(\phi)\frac{\partial \epsilon(\phi)}{\partial \phi_z}\right)_z\right]_{ijk}^n, \quad \frac{U_{ijk}^{n+1} - U_{ijk}^n}{\Delta t}$$
$$= D\nabla_d^2 U_{ijk}^n + \frac{\phi_{ijk}^{n+1} - \phi_{ijk}^n}{2\Delta t}, \tag{18}$$

where $\Delta_d U_{ijk}^n = (U_{i+1,jk}^n + U_{i-1,jk}^n + U_{i,j+1,k}^n + U_{i,j-1,k}^n + U_{ij,k+1}^n + U_{ij,k-1}^n - 6U_{ijk}^n)/h^2$. The curvature term $\left[\nabla_d \cdot (\epsilon^2(\phi)\nabla_d \phi)\right]_{ijk}^n$ in Eq. (17) is defined as follows:

$$\left[\nabla_d \cdot (\epsilon^2(\phi)\nabla_d \phi)\right]_{ijk}^n = \frac{\left[\epsilon^2(\phi_{i+1,jk}^n) + \epsilon^2(\phi_{ijk}^n)\right]\left(\phi_{i+1,jk}^n - \phi_{ijk}^n\right) - \left[\epsilon^2(\phi_{ijk}^n) + \epsilon^2(\phi_{i-1,jk}^n)\right]\left(\phi_{ijk}^n - \phi_{i-1,jk}^n\right)}{2h^2}$$
$$+ \frac{\left[\epsilon^2(\phi_{i,j+1,k}^n) + \epsilon^2(\phi_{ijk}^n)\right]\left(\phi_{i,j+1,k}^n - \phi_{ijk}^n\right) - \left[\epsilon^2(\phi_{ijk}^n) + \epsilon^2(\phi_{i,j-1,k}^n)\right]\left(\phi_{ijk}^n - \phi_{i,j-1,k}^n\right)}{2h^2}$$
$$+ \frac{\left[\epsilon^2(\phi_{ij,k+1}^n) + \epsilon^2(\phi_{ijk}^n)\right]\left(\phi_{ij,k+1}^n - \phi_{ijk}^n\right) - \left[\epsilon^2(\phi_{ijk}^n) + \epsilon^2(\phi_{ij,k-1}^n)\right]\left(\phi_{ijk}^n - \phi_{ij,k-1}^n\right)}{2h^2},$$

where the anisotropic function for cubic symmetry is discretized as follows:

$$\epsilon(\phi_{ijk}^n) = (1 - 3\delta_4)\left(1 + \frac{4\delta_4}{1-3\delta_4}\frac{(\phi_{i+1,jk}^n - \phi_{i-1,jk}^n)^4 + (\phi_{i,j+1,k}^n - \phi_{i,j-1,k}^n)^4 + (\phi_{ij,k+1}^n - \phi_{ij,k-1}^n)^4}{[(\phi_{i+1,jk}^n - \phi_{i-1,jk}^n)^2 + (\phi_{i,j+1,k}^n - \phi_{i,j-1,k}^n)^2 + (\phi_{ij,k+1}^n - \phi_{ij,k-1}^n)^2]^2}\right).$$

Let $\mathbf{m}_{i+\frac{1}{2},j+\frac{1}{2},k+\frac{1}{2}} = \left(m_{i+\frac{1}{2},j+\frac{1}{2},k+\frac{1}{2}}^x, \quad m_{i+\frac{1}{2},j+\frac{1}{2},k+\frac{1}{2}}^y, \quad m_{i+\frac{1}{2},j+\frac{1}{2},k+\frac{1}{2}}^z\right)$ be the gradient of ϕ at $(x_{i+\frac{1}{2}}, y_{j+\frac{1}{2}}, z_{k+\frac{1}{2}})$. The discretization of the curvature term $\left[\epsilon^2(\phi)|\nabla_d \phi|\nabla_d \cdot (\nabla_d \phi/|\nabla_d \phi|)\right]_{ijk}^n$ in Eq. (17) can be found in [37]. Finally the term $\left[\left(|\nabla \phi|^2 \epsilon(\phi)\partial \epsilon(\phi)/\partial \phi_x\right)_x\right]_{ijk}^n$ can be discretized as follows:

$$\left[\left(|\nabla \phi|^2 \epsilon(\phi)\frac{\partial \epsilon(\phi)}{\partial \phi_x}\right)_x\right]_{ijk}^n$$
$$= \left[\left(\frac{16\delta_4 \epsilon(\phi)\phi_x(\phi_x^2\phi_y^2 + \phi_x^2\phi_z^2 - \phi_y^4 - \phi_z^4)}{|\nabla \phi|^4}\right)_x\right]_{ijk}^n$$
$$= \frac{1}{2h}\left[\left(\frac{16\delta_4 \epsilon(\phi)\phi_x(\phi_x^2\phi_y^2 + \phi_x^2\phi_z^2 - \phi_y^4 - \phi_z^4)}{|\nabla \phi|^4}\right)_{i+1,jk}^n\right.$$
$$\left. - \left(\frac{16\delta_4 \epsilon(\phi)\phi_x(\phi_x^2\phi_y^2 + \phi_x^2\phi_z^2 - \phi_y^4 - \phi_z^4)}{|\nabla \phi|^4}\right)_{i-1,jk}^n\right], \tag{19}$$

where the partial derivatives are defined using the cell-centered finite difference method; $\left[\left(|\nabla \phi|^2 \epsilon(\phi)\partial \epsilon(\phi)/\partial \phi_y\right)_y\right]_{ijk}^n$ and $\left[\left(|\nabla \phi|^2 \epsilon(\phi)\partial \epsilon(\phi)/\partial \phi_z\right)_z\right]_{ijk}^n$ are similarly defined.

4. Numerical experiments

Now, we compare the computational results of dendritic growth in 2D and 3D spaces between the conventional and proposed phase-field models. Firstly, we simply test the curvature effect on crystal growth taking no consideration of temperature. Then k-fold symmetric crystal structure are used to specify the effect of artificial curvature on dendritic growth. And the polycrystal growth in undercooling liquid simulated by our proposed model is verified. Finally we perform the comparison test in three-dimensional space and give the sensitivity analysis of parameters which are used in the proposed model.

4.1. Curvature effect on growth

First, let us consider the artificial curvature effect on crystal growth. To highlight this effect, let us assume $\lambda = 0$ in the conventional phase-field Eq. (4), then it becomes

$$\epsilon^2(\theta)\frac{\partial \phi}{\partial t} = \nabla \cdot (\epsilon^2(\theta)\nabla \phi) + \phi(1-\phi^2) - \left(\epsilon'(\theta)\epsilon(\theta)\phi_y\right)_x$$
$$+ \left(\epsilon'(\theta)\epsilon(\theta)\phi_x\right)_y \tag{20}$$

and the proposed phase-field Eq. (9) becomes
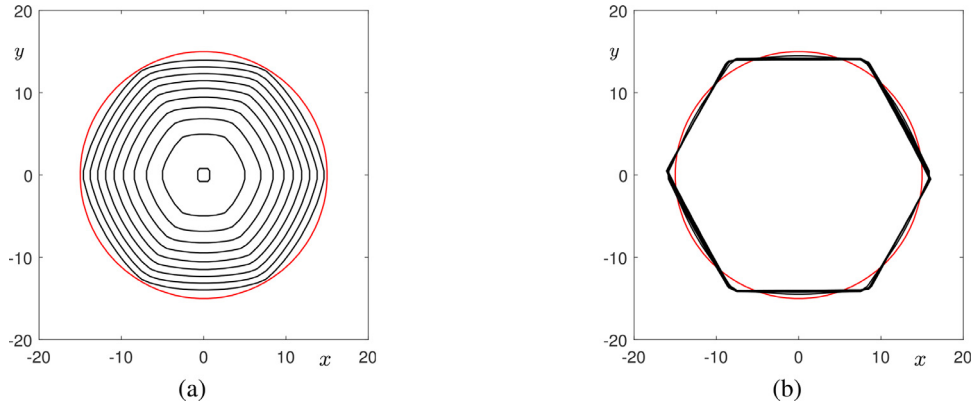
Fig. 2. Numerical results: (a) with artificial curvature effect and (b) without artificial curvature effect. Here, $\lambda = 0$ is used.

$$\epsilon^2(\theta)\frac{\partial\phi}{\partial t} = \nabla\cdot(\epsilon^2(\theta)\nabla\phi) - \epsilon^2(\theta)|\nabla\phi|\nabla\cdot\left(\frac{\nabla\phi}{|\nabla\phi|}\right)$$
$$+\phi(1-\phi^2) - \left(\epsilon'(\theta)\epsilon(\theta)\phi_y\right)_x + \left(\epsilon'(\theta)\epsilon(\theta)\phi_x\right)_y. \tag{21}$$

Assumed that the initial conditions on the computational domain $\Omega = (-20, 20) \times (-20, 20)$ are given as

$$\phi(x, y, 0) = \tanh\left(\frac{15 - \sqrt{x^2+y^2}}{\sqrt{2}}\right)$$

$$\text{and } U(x, y, 0) = \Delta\left(\frac{1 - \phi(x, y, 0)}{2}\right). \tag{22}$$

Here, $h = 1$, $\Delta t = 0.1h^2$, $\epsilon_0 = 1$, $k = 6$, $\Delta = -0.45$, and $\epsilon_6 = 1/(k^2 - 1) = 1/35$ are used.

Figure 2 (a) and (b) display the temporal evolution of the interface with and without artificial curvature effect, respectively. The interface is plotted at every 115 temporal iterations. When $\lambda = 0$, there is no growth factor and the growth of the crystal should stop. However, in the case of the conventional phase-field model, the crystal shrinks and finally disappears due to the artificial curvature effect as shown in Fig. 2(a). On the contrary, Fig. 2(b) shows the steady shape of the interfaces in the case of the proposed phase-field model without the artificial curvature effect. The crystal does not shrink and keeps the initial area and forms a six-fold symmetric interface as time evolves. Thus when the growth factor is not considered, if we want to keep the crystal shapes as the original, we should remove the artificial curvature term.
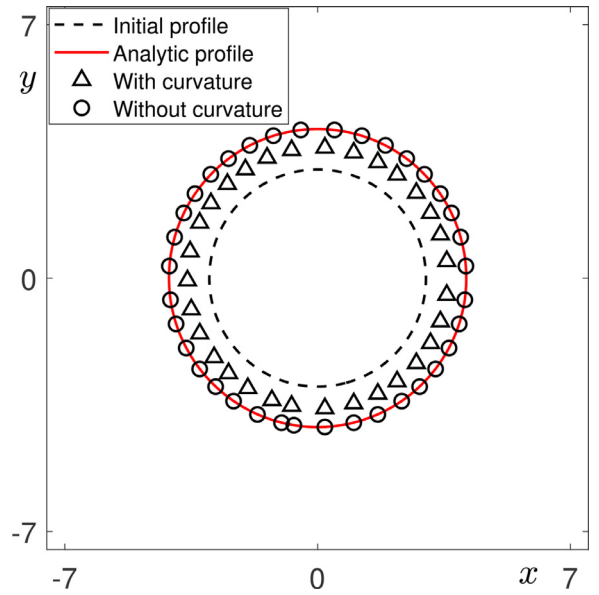
To validate the accuracy of the proposed model which has no curvature effect, we present a comparison test using the conventional and proposed models. For simplicity, we suppose isotropic crystal, i.e., $\epsilon = 1$ and constant temperature $U = \Delta$. Then, a reference governing equation becomes

$$\frac{\partial\phi}{\partial t} = -\lambda\Delta(1 - \phi^2)^2. \tag{23}$$

We solve the ordinary differential equation (ODE) (23) using the four-order Runge–Kutta method. The following Eqs. (24) and (25) represent the governing models with and without curvature effect, respectively.

$$\frac{\partial\phi}{\partial t} = \nabla^2\phi - |\nabla\phi|\nabla\cdot\left(\frac{\nabla\phi}{|\nabla\phi|}\right) + [\phi - \lambda\Delta(1-\phi^2)](1-\phi^2), \tag{24}$$

$$\frac{\partial\phi}{\partial t} = \nabla^2\phi + [\phi - \lambda\Delta(1-\phi^2)](1-\phi^2). \tag{25}$$

Fig. 3. Numerical comparison of the conventional and proposed models for the curvature effect.

For the comparison test, we set the parameters as $h = 2/15$, $\Delta t = 0.1h^2$, $\lambda = 1$, and $\Delta = -0.55$. Given initial condition on $\Omega = (-10, 10) \times (-10, 10)$ is as follow:

$$\phi(x, y, 0) = \frac{\tanh(3 - \sqrt{x^2+y^2})}{\sqrt{2}}. \tag{26}$$

Figure 3 illustrates the zero-level contours of the numerical solutions of the conventional and proposed models with the initial and reference solution at time $t = 1000\Delta t$. We can find that the solution of the proposed model, which is without the curvature effect, follows the reference solution profile well.

4.2. k-fold symmetric dendritic growth

Let us consider the anisotropic function $\epsilon(\phi) = \epsilon_0(1 + \epsilon_k\cos(k\phi))$ and perform comparison tests based on the k-fold crystal growth for $k = 4$ and 6. In this simulation, we use $N_x = N_y = 200$ on the computational domain $\Omega = (-70, 70) \times (-70, 70)$, $\lambda = 3.1913$, $D = 0.6267\lambda$, $\Delta = -0.55$, $\Delta t = 0.1h^2/D$, $\epsilon_k = 1/(k^2 - 1)$, and $\epsilon_0 = 1$. The initial condition
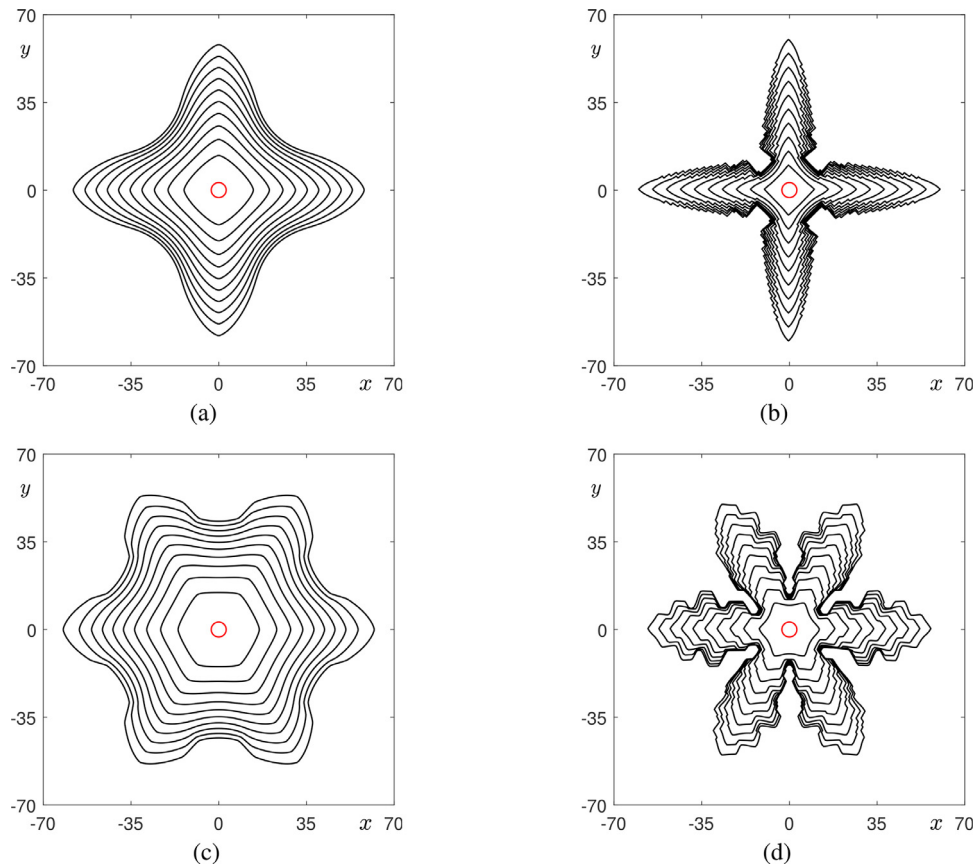
Fig. 4. (a)–(d) are snapshots of the temporal evolutions of the contours of ϕ at level zero up to times $t = 10,000\Delta t$, $3000\Delta t$, $16000\Delta t$, and $6000\Delta t$, respectively: (a) and (b) are the results with $k = 4$; (c) and (d) are the results with $k = 6$; (a) and (c) are the results with the conventional model; and (b) and (d) are the results with the proposed model without artificial curvature effect.

with a circle with radius $R = 3$ is taken as:

$$\phi(x, y, 0) = \tanh\left(\frac{R - \sqrt{x^2 + y^2}}{\sqrt{2}}\right)$$

$$\text{and } U(x, y, 0) = \Delta\left(\frac{1 - \phi(x, y, 0)}{2}\right). \quad (27)$$

Figure 4 (a)–(d) are snapshots of the temporal evolutions of the contours of ϕ at level zero up to the times $t = 10,000\Delta t$, $3000\Delta t$, $16000\Delta t$ and $6000\Delta t$, respectively. (a) and (b) are the results with $k = 4$; (c) and (d) are the results with $k = 6$; (a) and (c) are the results with the conventional model; and (b) and (d) are the results with the proposed model without artificial curvature effect. We should note that the final times are different in the four cases. From Fig. 4 we can see that in the case of the proposed phase-field model, the dendritic structure grows faster compared with the conventional model.

Figure 5 (a) and (b) display the overlapped contours for the results at the same time obtained from the conventional model (dashed line) and the proposed model without artificial curvature effect (solid line) for $k = 4$ and $k = 6$, respectively. It can be seen that the dendritic structure obtained from the proposed model develops much faster than that obtained from the conventional phase-field model. This phenomenon is more noticeable in earlier times because the curvature of structural interface is larger when the size of initial circle is smaller. Figure 6 displays the snapshots of temporal evolutions of the profile ϕ at level zero with different values of $\Delta = -0.45, -0.55, -0.65$. We can see that the dendritic structure grows faster under large initial undercooling sizes.

### 4.3. Polycrystal growth in the undercooling liquid

In this section, the dendritic growth of polycrystal in undercooling liquid is considered [3,38]. This test aims to show our model is applicable to a physical problem. We use $N_x = N_y = 400$ on the computational domain $\Omega = (-140, 140) \times (-140, 140)$, $\Delta = -0.55$, $R = 5$, and the other parameters are the same as those in Section 4.2 unless specified. The initial conditions are taken as:

$$\phi(x, y, 0) = \tanh\left(\frac{R - \sqrt{(x + x_0)^2 + (y + y_0)^2}}{\sqrt{2}}\right)$$

$$\text{and } U(x, y, 0) = \Delta\left(\frac{1 - \phi(x, y, 0)}{2}\right). \quad (28)$$

Firstly, we consider two crystals, whose distance between two circle centers is l. Here, $k = 4$ and $t = 5000\Delta t$ are taken. Figure 7(a), (b), and (c) show the polycrystal contours of ϕ at level zero obtained by our proposed model with $l = 20, 40$, and 100, respectively. It can be seen that if two crystals are nearby, the adjacent part of these two dendritic crystals stop growing, which results in the other part of dendritic crystals growing faster.

Next, different number of dendritic crystals growing in the undercooling liquid are performed. For two crystals, $(x_0, y_0) = (10.5, 0)$ and $(-10.5, 0)$. For three dendritic crystals, $(x_0, y_0) = (0, -12)$, $(10.5, 6)$ and $(-10.5, 6)$. For four dendritic crystals, $(x_0, y_0) = (10.5, -10.5)$, $(10.5, 10.5)$, $(-10.5, 10.5)$ and $(-10.5, -10.5)$. For five number of dendritic crystals, $(x_0, y_0) = (21, 2)$, $(10.5, -15.5)$, $(0, 13.5)$, $(-21, 2)$ and $(-10.5, -15.5)$. Here, $k = 4$ and $t = 5000\Delta t$ are used. Figure 8 shows the polycrystal contours of ϕ at level zero with different
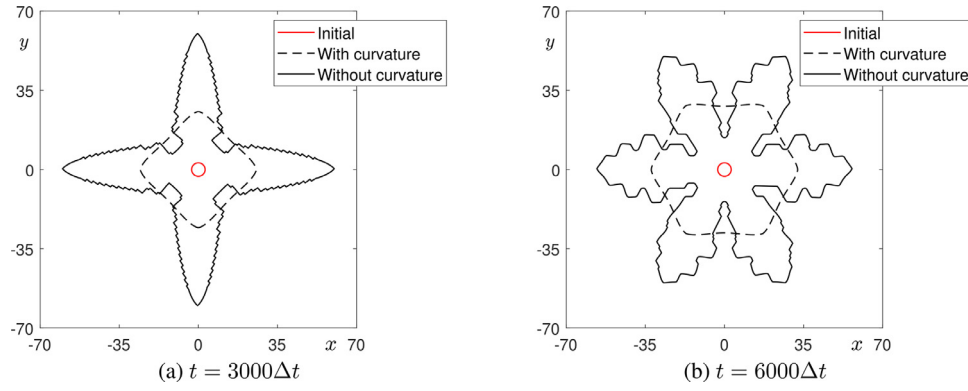
Fig. 5. Overlapped contours for the results from the conventional model (dashed line) and the proposed model without artificial curvature effect (solid line) for (a) $k = 4$ and (b) $k = 6$.
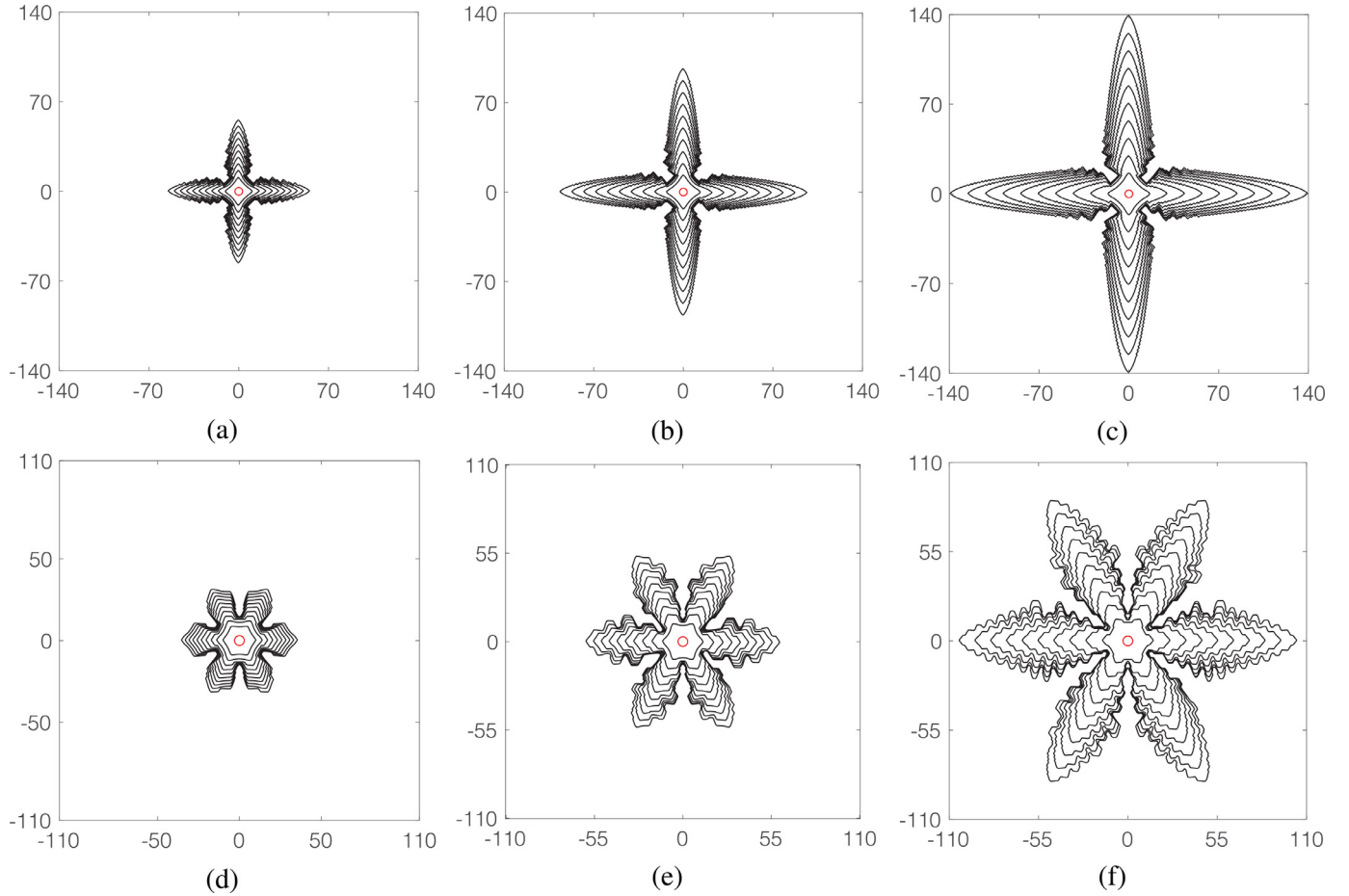
Fig. 6. The contours of ϕ at level zero for the proposed model with different initial undercooling sizes. The top row corresponds $k = 4$ at time $t = 5000\Delta t$ and the bottom row corresponds $k = 6$ at time $t = 6000\Delta t$. (a) and (d) are the results with $\Delta = -0.45$. (b) and (e) are the results with $\Delta = -0.55$. (c) and (f) are the results with $\Delta = -0.65$.

numbers of dendritic growth obtained by our model. We can find that the adjacent part of two or more dendritic crystals stop growing. The conclusion that some parts of too close crystals being stopped growing is irrelevant to the number of crystals can be obtained.

Finally, let us consider the effect of the angle rotation on the polycrystal growth. Assumed that the four circle centers in initial conditions are: $(x_0, y_0) = (25, -25), (-25, -25), (-25, 25)$ and $(25, 25)$ on four different quadrants respectively. The clockwise rotated angles are $0, \pi/4, \pi/2, 3\pi/4$ for these four crystals respectively. Here, $k = 6$ and $t = 6000\Delta t$ are taken. Figure 9(a) and
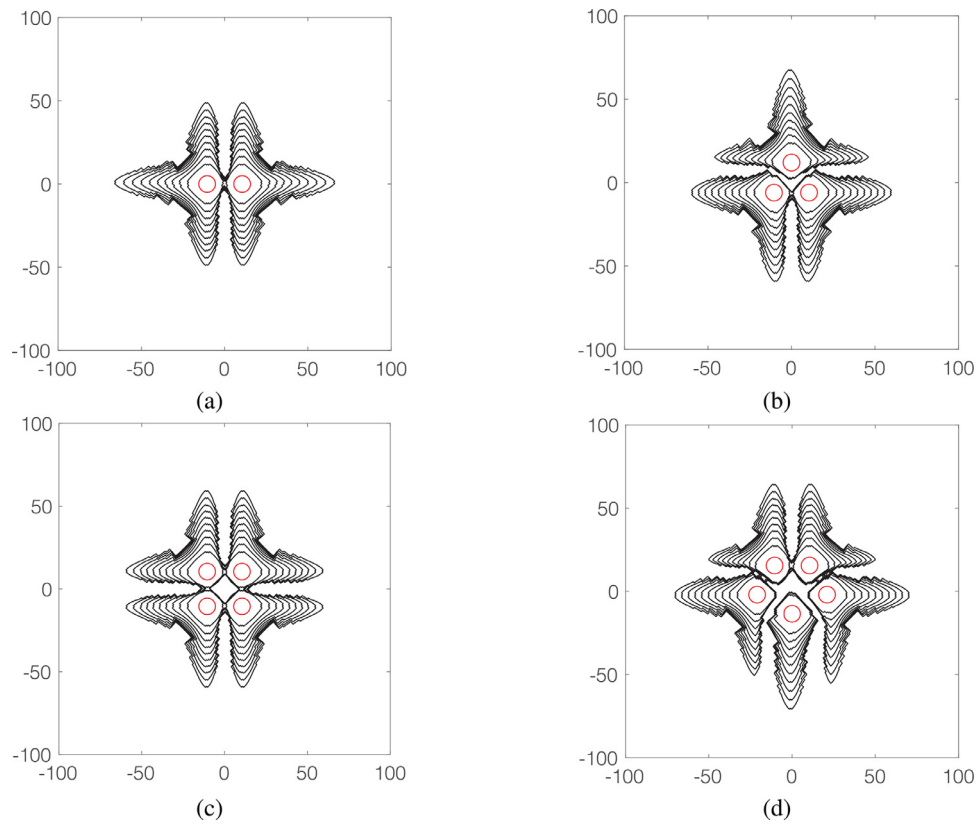
(b) show the polycrystal contours of the results from our proposed model before and after angle rotation. It can be seen that the growth orientation of polycrystal can change as θ rotates $0, \pi/4, \pi/2, 3\pi/4$ clockwise.

### 4.4. Three-dimensional crystal growth

Next, to highlight the difference of growth dynamics between the conventional and proposed phase-field models in 3D space, we perform some computational tests for dendritic growth in 3D space. In this three-dimensional simulation, we use $N_x = N_y = N_z = 200$ in the computational domain $\Omega = (-80, 80) \times (-80, 80) \times$
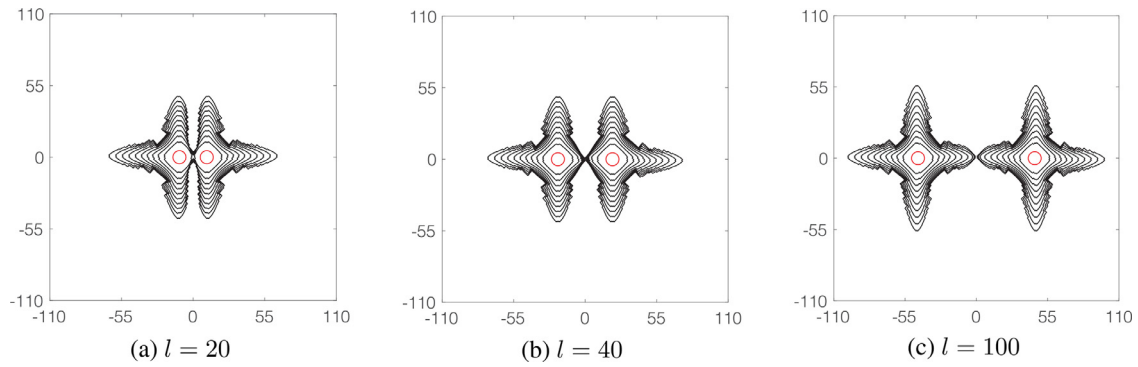
Fig. 7. Polycrystal contours for the results from the proposed model without artificial curvature effect. l represents the distance between two circle centers. Here, $k = 4$, $\Delta = -0.55$ and $t = 5000\Delta t$ are used.


Fig. 8. Polycrystal contours of ϕ at level zero obtained from our proposed model with different number of crystals. Here $k = 4$, $\Delta = -0.55$ and $t = 5000\Delta t$ are used.
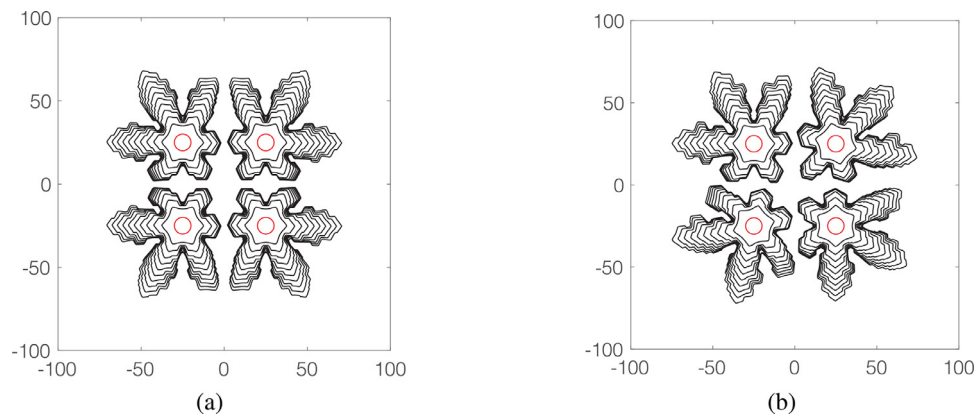

Fig. 9. Polycrystal contours for the results from the proposed model without artificial curvature effect. (a) is the results before rotation and (b) is the result after θ of the four crystals rotating $0, \pi/4, \pi/2, 3\pi/4$ clockwise. Here, $k = 6$, $\Delta = -0.55$ and $t = 6000\Delta t$ are used.
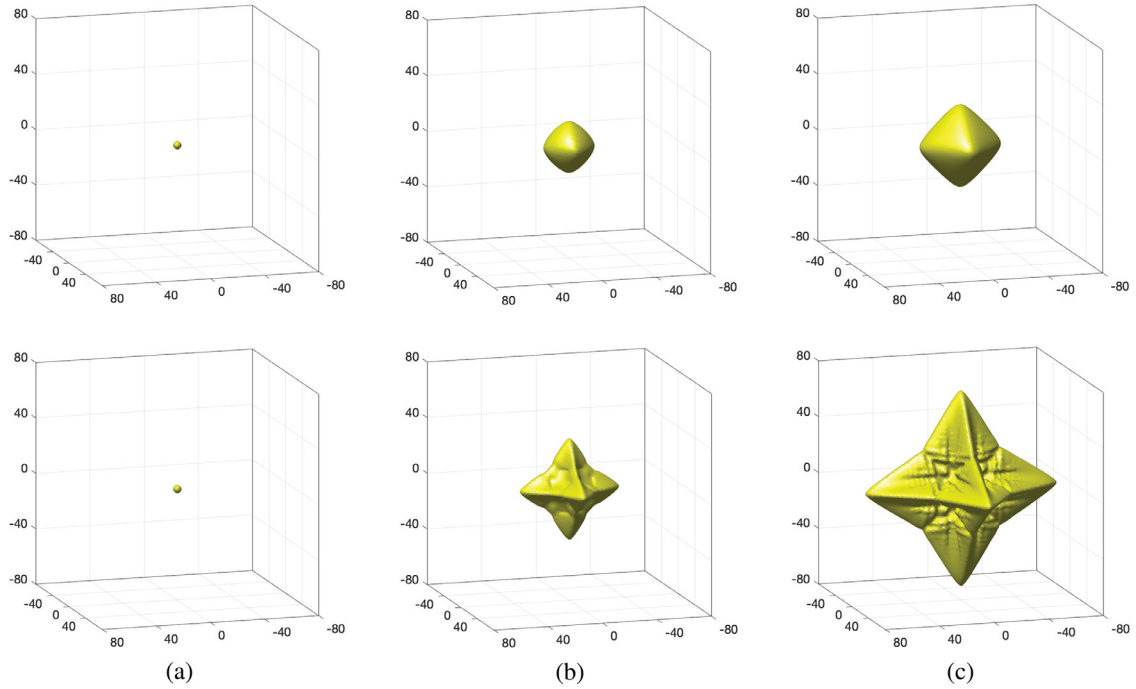
Fig. 10. Temporal evolution of the isosurface of ϕ at level zero for the conventional model (top row) and the proposed model (bottom row). Here, (a), (b) and (c) are the results at times $t = 0$, $1000\Delta t$, $2000\Delta t$, respectively.
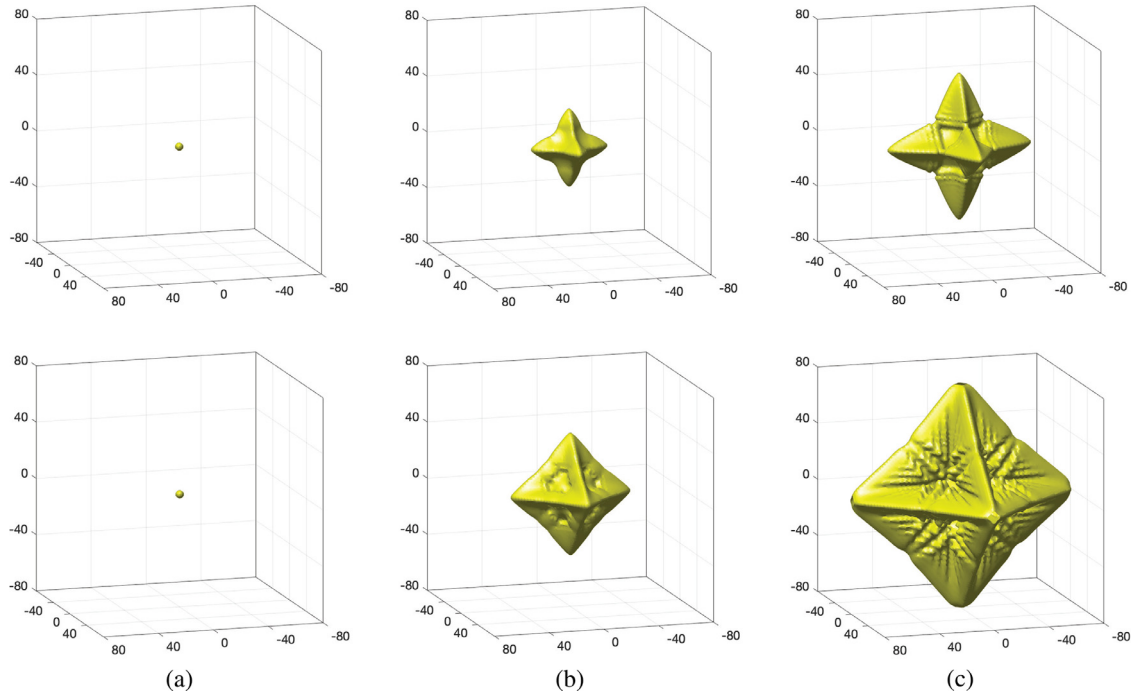

Fig. 11. Temporal evolution of the isosurface of ϕ at level zero for the proposed model with $\Delta = -0.45$ (top row) and $\Delta = -0.65$ (bottom row). Here, (a), (b), and (c) are the results at times $t = 0$, $1000\Delta t$, $2000\Delta t$, respectively.

$(-80, 80)$ and we take $\delta_4 = 0.05$, $D = 2$, $\lambda = 1.5957D$, $\Delta = -0.55$, and $\Delta t = 0.1h^2/D$. The initial conditions are taken as $\phi(x, y, z, 0) = \tanh\left[(R - \sqrt{x^2 + y^2 + z^2})/\sqrt{2}\right]$ where $R = 3$ is the initial radius of ball; $U(x, y, z, 0) = 0$ if $\phi(x, y, z, 0) > 0$ and $U(x, y, z, 0) = \Delta$ otherwise.

Figure 10(a), (b), and (c) display the temporal evolution of the isosurface of ϕ at level zero for the conventional model (top row) and the proposed model (bottom row) at times $t = 0$, $1000\Delta t$,

$2000\Delta t$, respectively. It can be seen that the three-dimensional dendritic structure obtained from the proposed model develops much faster than that obtained from the conventional phase-field model. This phenomenon is more noticeable in earlier times because the curvature of interface is larger when the size of initial ball is smaller. Because dendritic structure forms faster than the conventional phase-field model does, the proposed phase-field model has the advantage of less CPU computing time and reduced more memory. Therefore, if we use the proposed phase-field
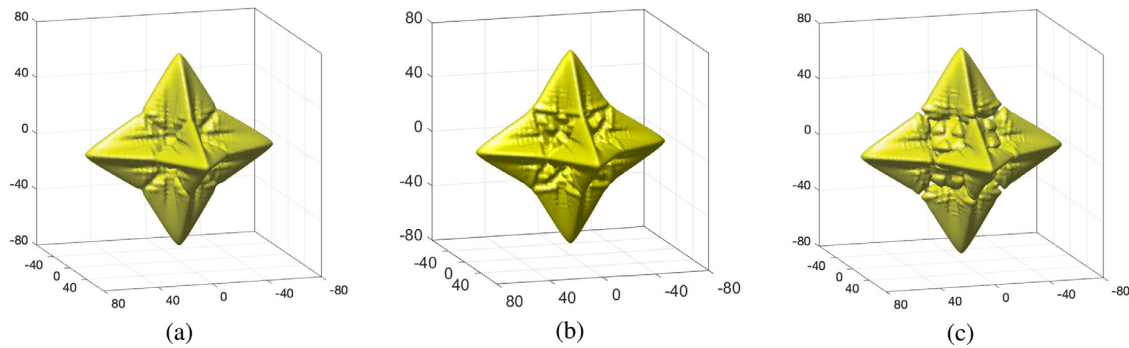
Fig. 12. The isosurface of ϕ at level zero for the proposed model with different initial radius at time $t = 2000\Delta t$. From left to right, $R = 1, 5, 10$ respectively. Here, $\Delta = -0.55$.

model, we can obtain a much detailed dendritic structure under the equivalent computational resources used by the conventional phase-field model.

4.5. Effect of initial undercooling sizes and radius in 3D dendritic growth

Next, we study the effects of the initial undercooling sizes Δ and the initial radius of ball R on the growth of dendritic structure in our proposed model. Figure 11 shows sequences of isosurfaces ϕ at level zero with different undercooling sizes $\Delta = -0.45$ (top row) and $\Delta = -0.65$ (bottom row) at times $t = 0$, $1000\Delta t$, $2000\Delta t$. It can be observed that the dendritic structure grows faster under the large initial undercooling size. Figure 12(a), (b) and (c) show the isosurfaces of ϕ at level zero at time $t = 2000\Delta t$ for the proposed model with the initial radius of ball $R = 1, 10, 20$ respectively. We can see that the dendritic structure become fatter with the large radius of initial ball. Therefore, we can utilize the initial undercooling size Δ and the radius R in the proposed model to control the dendritic crystal growth speed.

5. Conclusions

In this article, we presented a novel phase-field model without artificial curvature effect for the crystal growth simulation. The numerical experiments highlighted the difference between the computational results from the proposed and conventional phase-field models for dendritic growth simulation. In the case of the new phase-field model without the artificial curvature effect in both the two-dimensional and three-dimensional spaces, dendritic growth developed faster than that in the case of the conventional phase-field model because the new model reduces the artificial curvature effect. Our proposed model was also applicable to polycrystal growth in undercooling liquid. In this study, to focus on the novel phase-field model, we used the simple explicit numerical scheme for the proposed model. In the future work, we will further investigate high-order accurate and more stable numerical schemes such as that proposed by Zhang and Yang [39] for the phase-field model without the artificial curvature effect. Furthermore, the proposed crystal growth model can be coupled with a momentum equation of fluid flow for simulating dendritic growth with convection [40–42].

Declaration of Competing Interest

The authors declare that they have no known competing financial interests or personal relationships that could have appeared to influence the work reported in this paper.

CRediT authorship contribution statement

Yibao Li: Conceptualization, Validation, Formal analysis, Investigation, Writing – original draft, Visualization, Funding acquisition. **Qian Yu:** Software, Validation, Investigation, Formal analysis, Writing – original draft, Visualization. **Seokjun Ham:** Software, Validation, Investigation, Writing – original draft, Writing – review & editing, Visualization. **Soobin Kwak:** Validation, Data curation, Writing – original draft. **Chaeyoung Lee:** Formal analysis, Software, Writing – original draft. **Junseok Kim:** Conceptualization, Methodology, Resources, Writing – original draft, Writing – review & editing, Supervision, Project administration, Funding acquisition.

Data availability

No data was used for the research described in the article.

Acknowledgment

References

[1] W. Chen, Y. Zhao, S. Yang, D. Zhang, H. Hou, Three-dimensional phase-field simulations of the influence of diffusion interface width on dendritic growth of Fe-0.5 wt.% C alloy, Adv. Compos. Hybrid Mater. 4 (2) (2021) 371–378.

[2] L. Guangguang, L. Sen, W. Zhaohui, W. Weiling, Z. Miaoyong, W. Xiaohua, Phase-field simulation for non-isothermal solidification of Al-Cu binary alloy, Mater. Res. (2019) 22.

[3] B. Xia, C. Mei, Q. Yu, Y. Li, A second order unconditionally stable scheme for the modified phase field crystal model with elastic interaction and stochastic noise effect, Comput. Methods Appl. Mech. Eng. 363 (2020) 112795.

[4] T. Kishimoto, Y. Sekozawa, H. Yamazaki, H. Murakawa, K. Kuchitsu, M. Ishikawa, Seasonal changes in ice nucleation activity in blueberry stems and effects of cold treatments in vitro, Environ. Exp. Bot. 106 (2014) 13–23.

[5] X. Zhang, Y. Wang, D. Liu, Z. Ji, H. Xu, M. Hu, P. Cui, Effect of stirring rate on grain morphology of Mg-Al alloy semi-solid structure by phase field lattice Boltzmann simulation, J. Cryst. Growth 543 (2020) 125704.

[6] I.B. Sebastião, B. Bhatnagar, S. Tchessalov, S. Ohtake, M. Plitzko, B. Luy, A. Alexeenko, Bulk dynamic spray freeze-drying Part 1: modeling of droplet cooling and phase change, J. Pharm. Sci. 108 (6) (2019) 2063–2074.

[7] R. Kobayashi, Modeling and numerical simulations of dendritic crystal growth, Physica D 63 (3–4) (1993) 410–423.

[8] R. Kobayashi, A numerical approach to three-dimensional dendritic solidification, Exp. Math. 3 (1) (1994) 59–81.

[9] N. Ren, J. Li, N. Bogdan, M. Xia, J. Li, Simulation of dendritic remelting and fragmentation using coupled cellular automaton and Eulerian multiphase model, Comput. Mater. Sci 180 (2020) 109714.

[10] W. Lee, Y. Jeong, J.W. Lee, H. Le, S.H. Kang, Y.M. Kim, J. Yoon, Numerical simulation for dendrite growth in directional solidification using LBM-CA (cellular automata) coupled method, J. Mater. Sci. Technol. 49 (2020) 15–24.

[11] W. Zhao, Y.C. Hon, M. Stoll, Numerical simulations of nonlocal phase-field and hyperbolic nonlocal phase-field models via localized radial basis functions-based pseudo-spectral method (LRBF-PSM), Appl. Math. Comput. 337 (2018) 514–534.

[12] Q. Yu, K. Wang, B. Xia, Y. Li, First and second order unconditionally energy stable schemes for topology optimization based on phase field method, Appl. Math. Comput. 405 (2021) 126267.

[13] G. Demange, H. Zapolsky, R. Patte, M. Brunel, A phase field model for snow crystal growth in three dimensions, npj Comput. Mater. 3 (1) (2017) 1–7.

[14] X. Yang, Fully-discrete spectral-Galerkin scheme with decoupled structure and second-order time accuracy for the anisotropic phase-field dendritic crystal growth model, Int. J. Heat Mass Transf. 180 (2021) 121750.

[15] S. Lee, D. Lee, The fractional Allen–Cahn equation with the sextic potential, Appl. Math. Comput. 351 (2019) 176–192.

[16] H.G. Lee, High-order and mass conservative methods for the conservative Allen–Cahn equation, Comput. Math. Appl. 72 (3) (2016) 620–631.

[17] Z. Weng, L. Tang, Analysis of the operator splitting scheme for the Allen–Cahn equation, Numer. Heat Transf. Part B Fundamentals 70 (5) (2016) 472–483.

[18] Y. Gong, J. Zhao, Q. Wang, Arbitrarily high-order unconditionally energy stable SAV schemes for gradient flow models, Comput. Phys. Commun. 249 (2020) 107033.

[19] T. Takaki, J. Kato, Phase-field topology optimization model that removes the curvature effects, Mech. Eng. J. (2017) 16–00462.

[20] P.H. Chiu, Y.T. Lin, A conservative phase field method for solving incompressible two-phase flows, J. Comput. Phys. 230 (1) (2011) 185–204.

[21] S. Aihara, T. Takaki, N. Takada, Multi-phase-field modeling using a conservative Allen–Cahn equation for multiphase flow, Comput. Fluids 178 (2019) 141–151.

[22] Y. Hu, D. Li, Q. He, Generalized conservative phase field model and its lattice Boltzmann scheme for multicomponent multiphase flows, Int. J. Multiphase Flow 132 (2020) 103432.

[23] J. Yang, Y. Li, C. Lee, J. Kim, Conservative Allen–Cahn equation with a nonstandard variable mobility, Acta Mech. 231 (2) (2020) 561–576.

[24] Q. Li, T. Zhang, J. Yuan, Numerical simulation of polymer crystal growth under flow field using a coupled phase-field and lattice Boltzmann method, Appl. Math. Comput. 387 (2020) 124302.

[25] N. Wang, D. Korba, Z. Liu, R. Prabhu, M.W. Priddy, S. Yang, L. Li, Phase-field-lattice Boltzmann method for dendritic growth with melt flow and thermosolutal convection–diffusion, Comput. Methods Appl. Mech. Eng. 385 (2021) 114026.

[26] A. Shah, M. Sabir, P. Bastian, An efficient time-stepping scheme for numerical simulation of dendritic crystal growth, Eur. J. Comput. Mech. 25 (6) (2016) 475–488.

[27] J. Wu, Z. Guo, C. Luo, Development of a parallel adaptive multigrid algorithm for solving the multi-scale thermal-solute 3D phase-field problems, Comput. Mater. Sci 142 (2018) 89–98.

[28] M.H. Chen, P.C. Bollada, P.K. Jimack, Dynamic load balancing for the parallel, adaptive, multigrid solution of implicit phase-field simulations, Int. J. Numer. Anal. Model. 16 (2) (2019) 297–318.

[29] Y. Li, H.G. Lee, J. Kim, A fast, robust, and accurate operator splitting method for phase-field simulations of crystal growth, J. Cryst. Growth 321 (1) (2011) 176–182.

[30] J.W.J. Kaiser, S. Adami, I.S. Akhatov, N.A. Adams, A semi-implicit conservative sharp-interface method for liquid-solid phase transition, Int. J. Heat Mass Transf. 155 (2020) 119800.

[31] A. Zhang, J. Du, Z. Guo, Q. Wang, S. Xiong, Evolution of specific interface area during solidification: a three-dimensional thermosolutal phase-field study, Comput. Phys. Commun. 267 (2021) 108042.

[32] S. Nandi, Y.V.S.S. Sanyasiraju, A grid based ADI method for the problem of two phase solidification, Int. J. Heat Mass Transf. 178 (2021) 121569.

[33] G. Grinstein, G. Mazenko, Directions in Condensed Matter Physics: Memorial Volume in Honor of Prof. S.K. Ma, World Scientific, Singapore; Philadelphia, PA, 1986.

[34] S. Lee, Y. Li, J. Shin, J. Kim, Phase-field simulations of crystal growth in a two-dimensional cavity flow, Comput. Phys. Commun. 216 (2017) 84–94.

[35] S. Zhao, X. Xiao, X. Feng, An efficient time adaptivity based on chemical potential for surface Cahn–Hilliard equation using finite element approximation, Appl. Math. Comput. 369 (2020) 124901.

[36] D. Jeong, J. Kim, Fast and accurate adaptive finite difference method for dendritic growth, Comput. Phys. Commun. 236 (2019) 95–103.

[37] S.D. Yang, H.G. Lee, J. Kim, A phase-field approach for minimizing the area of triply periodic surfaces with volume constraint, Comput. Phys. Commun. 181 (6) (2010) 1037–1046.

[38] Y. Li, J. Kim, An efficient and stable compact fourth-order finite difference scheme for the phase field crystal equation, Comput. Methods Appl. Mech. Eng. 319 (2017) 194–216.

[39] J. Zhang, X. Yang, A fully decoupled, linear and unconditionally energy stable numerical scheme for a melt-convective phase-field dendritic solidification model, Comput. Methods Appl. Mech. Eng. 363 (2020) 112779.

[40] D. Sun, H. Xing, X. Dong, Y. Han, An anisotropic lattice Boltzmann–phase field scheme for numerical simulations of dendritic growth with melt convection, Int. J. Heat Mass Transf. 133 (2019) 1240–1250.

[41] T.Z. Gong, Y. Chen, D.Z. Li, Y.F. Cao, P.X. Fu, Quantitative comparison of dendritic growth under forced flow between 2D and 3D phase-field simulation, Int. J. Heat Mass Transf. 135 (2019) 262–273.

[42] J.Q. Li, T.H. Fan, Phase-field modeling of macroscopic freezing dynamics in a cylindrical vessel, Int. J. Heat Mass Transf. 156 (2020) 119915.